 doi:10.20944/preprints202110.0174.v1

Article

Bragg Mirrors for Thermal Waves.

A. Camacho de la Rosa [1,‡], D. Becerril [2,‡], G. Gómez-Farfán [1,‡] and R. Esquivel-Sirvent [1,‡*] 0000-0002-8168-180X

[1] Instituto de Física, Universidad Nacional Autónoma de México, Apartado Postal 20-364, Ciudad de México, 01000, Mexico.
[2] Istituto di Struttura della Materia, CNR, Via Fosso del Cavaliere 100, 00133 Rome, Italy.
* Correspondence: raul@fisica.unam.mx
‡ These authors contributed equally to this work.

Abstract: We present a numerical calculation of the heat transport in a Bragg mirror configuration made of materials that do not obey Fourier's law of heat conduction. The Bragg mirror is made of materials that are described by the Cattaneo-Vernotte equation. By analyzing the Cattaneo-Vernotte equation's solutions, we define the thermal wave surface impedance to design highly reflective thermal Bragg mirrors. Even for mirrors with a few layers, very high reflectance is achieved ($> 90\%$). The Bragg mirror configuration is also a system that makes evident the wave-like nature of the solution of the Cattaneo-Vernotte equation by showing frequency pass-bands that are absent if the materials obey the usual Fourier's law.

Keywords: Cattaneo-Vernotte; waves; Bragg.

1. Introduction

The assumption of a causal response in the Fourier law of heat transport, introduces a time delay between the temperature gradient and the heat flux. This time delay implies a finite velocity of heat propagation, and the temperature and heat flux obey a hyperbolic partial differential equation known as the Cattaneo-Vernotte equation (CVe) [1–5]. As a hyperbolic equation its solutions are wave-like and it is possible to have heat or temperature waves that satisfy particular dispersion relations [6,7].

Several experiments have explored the non-Fourier behavior of heat transport in a variety of systems, like granular media [3,8], wet sands [9], organic materials [10], blood and porcine muscle [11], and processed meat [12]. Skin bio-thermomechanics and bioheat transfer mechanisms also follow a non-Fourier behavior [13–15]. Recently the wave-like behavior was shown experimentally in bulk Ge for temperatures between 7 K to room temperature, opening new potential applications for heat waves [16].

For wave-like behavior, proposals to control the heat flux have been reported which are inspired by systems similar to those used in optics or acoustics. For example, thermal cloaking from coated spheres mimicking a metamaterial has been proposed [17] as well as thermal or temperonic crystals [18,19]. The latter are made of an array of layers forming a periodic one-dimensional system or superlattice. Similar work was done by Gandolfi using a dual-phase lag equation that introduces an extra term (third order derivative of the temperature) in the CVe [19]. Previously, the CVe was solved for a layered system under a pulsed heat source determining the effective or average thermal properties [20]. Chen [18] uses the CVe in a superlattice and calculates the dispersion relation using Bloch's theorem. Ballistic-diffusive models for heat transport in superlattice using the Guyer-Krumhansl equation since the thickness of the layers is comparable to the mean free path of the phonons [21].

Superlattices have the advantage of being simple to fabricate and experimentally characterize. Their use in heat transport has been limited to the case of Fourier heat conduction. Using a periodic structure of alternate layers of porous Si, due to the ensuing photonic band structure, it is possible to show that heating in the light band gaps

Preprints (www.preprints.org) | NOT PEER-REVIEWED | Posted: 12 October 2021 doi:10.20944/preprints202110.0174.v1

decreases the temperature of the system [22,23]. The thermal conductivity of superlattices comprised of different semiconductors have been studied using the Boltzman transport equation and could have possible applications in thermoelectric and optoelectronic devices [24].

For a finite system, Bloch's theorem is no longer applicable, and while the presence of the bounding surfaces will break the periodicity, some of the main features of the infinite superlattice remain. For example, the reflectivity will show regions of high and low values in the frequency regions of the allowed and forbidden bands of the dispersion relation depending on the length of the superlattice [25–27]. The observed band gaps or quasi-band gaps are due to interference effects of the waves in the superlattice. A particularly useful finite system is a Bragg mirror made of alternate layers of high and low dielectric constants [28] or acoustic impedances [29,30].

In this paper, we demonstrate the possibility of Bragg mirrors for thermal waves that are solutions to the Cattaneo-Vernotte equation. The mirrors are made of alternate layers of two different materials with different thermal properties. Even for mirrors made of a few bilayers, a high reflection of the thermal waves is achieved. The changes in the heat flux into the Bragg mirror as a function of frequency, are only possible with wave-like behavior. Further refinement of the flux can be achieved by introducing defects into the mirror. Besides presenting a system to show the wave-like nature of the solution of the CVe, we discuss possible applications in heat management.

2. Thermal waves. Cattaneo-Vernotte equation

In this section we review the basic characteristics of *thermal waves* as solutions of the Cattaneo-Vernotte equation (CVe). Consider a medium with thermal conductivity κ [W m^{-1} K^{-1}], mass density ρ [kg m^{-3}] and specific heat capacity at constant volume c_v [J kg^{-1}K^{-1}]. The CVe arises when there is a time delay τ between the application of a temperature gradient $\nabla T(\vec{r},t)$ and the ensuing heat flux $\vec{q}(\vec{r},t)$, leading to the equation [1–4]

$$\vec{q}(\vec{r},t)+\tau\frac{\partial\vec{q}(\vec{r},t)}{\partial t}=-\kappa\nabla T(\vec{r},t). \tag{1}$$

Taking the divergence of Eq. (1) and considering the balance equation of the thermal energy density $u(\vec{r},t)$ without sources, given by $\rho c_v\dfrac{\partial T}{\partial t}+\nabla\cdot\vec{q}=0$ yields

$$\nabla^2T(\vec{r},t)=\frac{1}{\alpha}\frac{\partial T(\vec{r},t)}{\partial t}+\frac{1}{v^2}\frac{\partial^2T(\vec{r},t)}{\partial t^2}. \tag{2}$$

The thermal diffusivity is defined as $\alpha=\kappa/\rho c_v$. The parameter $v=\alpha/\tau$ is identified as the propagation speed of the thermal perturbation [31,32]. In the limit $\tau\to 0$, the speed v goes to infinity, and Eq. (1) reduces to the usual Fourier law for heat conduction [33–35].

Assuming a harmonic time-dependence, the solution of Eq. (2) is

$$T(\vec{r},t)=Ae^{i(\vec{k}\cdot\vec{r}-\omega t)}+Be^{-i(\vec{k}\cdot\vec{r}+\omega t)}, \tag{3}$$

where the complex wavevector is

$$|\vec{k}|=k=\sqrt{\left(\frac{\omega}{v}\right)^2+i\frac{\omega}{\alpha}}. \tag{4}$$

We point out two limits of interest: 1) when $\omega\tau<<1$, the CVe goes to the usual diffusion equation; and 2) when $\omega\tau\to\infty$, the wavenumber k becomes real and the temperature profile behaves as a non-damped wave equation.

From the wavenumber k Eq. (4), we define the penetration length as $\delta=1/\mathrm{Im}(k)$ and the wavelength is $\lambda=2\pi/\mathrm{Re}(k)$. For the CVe a characteristic length scale is $\ell=4\pi\alpha/\omega$ and we can write $\delta_{cv}=\ell^2/\lambda_{cv}$. If $0<\lambda<\ell$, then we are in a highly

Preprints (www.preprints.org) | NOT PEER-REVIEWED | Posted: 12 October 2021 doi:10.20944/preprints202110.0174.v1

damped regime. Otherwise, the wavelike behavior dominates with little damping. In the Fourier law, we have the relation $\delta_f = \lambda_f/2\pi$, which implies that penetration length is smaller than the wavelength and decreases before it reaches a period, thus the damped behavior dominates.

The heat flux for the CVe is obtained by replacing Eq. (3) in Eq. (1) as

$$\vec{q}(\vec{r},t) = -i\mathcal{K}(\omega)k\hat{k}\Big(Ae^{i(\vec{k}\cdot\vec{r}-\omega t)} - Be^{-i(\vec{k}\cdot\vec{r}+\omega t)}\Big), \tag{5}$$

where the modified thermal conductivity is given by $\mathcal{K}(\omega) = \frac{\kappa}{1-i\omega\tau}$. This allows us to define $Y(\omega) = -i\mathcal{K}(\omega)k$ as the *thermal admittance*, and it can be expressed as

$$Y(\omega) = \frac{\kappa}{v\tau}\frac{1}{\sqrt{1+i/\omega\tau}}. \tag{6}$$

The reciprocal of the admittance defines the *thermal impedance* [36], $Z_i(\omega) = T/\vec{q}_i \cdot \hat{n}$, where $\hat{n}$ is the normal vector to the i^{th} interface.

3. Thermal superlattice

Consider an array of N layers in a Cartesian coordinates system (x, y, z) where the x-axis is perpendicular to the interfaces. Each layer is of width d_j with thermal properties α_j, v_j. The first interface is at $x_0 = 0$ and the last layer interface is at $x_N = d_1 + \cdots + d_N = L$. Outside the layered structure, for $x < x_0$ there is a medium with thermal properties α_0, v_0; and for $x > x_N$ there is a substrate defined by α_s, v_s. We will consider normal incidence, thus $\vec{q}(\vec{r},t) = q(x,t)\hat{x}$.

Following the usual transfer matrix formalism the fields at the first interface $x = x_0$ are related to those at the final $x = x_L$ as:

$$\begin{pmatrix} T(L) \\ q(L) \end{pmatrix} = (M_N M_{N-1} ... M_1)\begin{pmatrix} T(0) \\ q(0) \end{pmatrix}. \tag{7}$$

Here the matrix M_j is given by [20,37]

$$M_j = \begin{pmatrix} \cos(k_j d_j) & -\frac{1}{Y_j}\sin(k_j d_j) \\ Y_j \sin(k_j d_j) & \cos(k_j d_j) \end{pmatrix}\begin{pmatrix} 1 & R_{j,j+1} \\ 0 & 1 \end{pmatrix}, \tag{8}$$

where $R_{j,j+1}$ is the interfacial or Kapitza resistance between the j^{th} and $j+1$ interfaces.

The matrix $M = \prod_{j=0}^{N-1} M_{N-j}$ in Eq. (7) is known as the associated transfer matrix which transfers the fields, in this case temperature and heat flux, through a given domain [38]. The reflection coefficient r for the finite system is expressed in terms of the surface admittance of the layered structure Y as follows [39]

$$r = \frac{Y_0 - Y}{Y_0 + Y}. \tag{9}$$

Here Y_0 is the admittance of the initial medium, Y is written in terms of the admittance of the substrate Y_s and the components of the associated transfer matrix as [38,39]

$$Y = \frac{M_{21} - Y_s M_{11}}{Y_s M_{12} - M_{22}}. \tag{10}$$

We will consider a Bragg mirror made by repeating a unit cell with two materials $m1$ and $m2$. If we have n unit cells the total transfer matrix is $M = (M_2 M_1)^n$. If the number of cells is infinite we obtain a superlattice with a translational invariance for $x > 0$.

We want to compare the reflectivity r of the finite and infinite superlattice. For the infinite case we use Bloch's theorem [18,19], which establishes the dispersion relation of

Preprints (www.preprints.org) | NOT PEER-REVIEWED | Posted: 12 October 2021 doi:10.20944/preprints202110.0174.v1

the Bloch wavenumber $\mathcal{Q}$ as $\cos(p\mathcal{Q}) = \frac{1}{2}Tr(M)$, where $p = d_1 + d_2$ is the period of the superlattice, and $M = M_2M_1$ is the transfer matrix of the unit cell. In the infinite case the reflectivity r will be given by Eq. (9) but with admittance

$$Y = \frac{M_{12}}{i(e^{i\mathcal{Q}p} - M_{11})}. \tag{11}$$

The calculation of the transfer matrix requires the values of the interfacial resistance. However the contribution is negligible for our particular problem. For the materials we discuss in this work, whose value can be similar to the contact between soft-matter or liquid-liquid interfaces [40,41] the values of the interfacial thermal conductance $G = 1/R$ are in the range $G \in [1.05, 3] \times 10^6$ $[Wm^{-2}K^{-1}]$. For these values the interfacial thermal resistance is negligible when calculating the total transfer matrix of the system. This is because the Kapitza length $l_k = \kappa R$ is much smaller than the thickness of the layers.

There is an important difference between the CVe and other wave phenomena, such as electromagnetic or acoustic. The reflectance is defined as the ratio of the reflected power to the incident power of a wave [42]. For example, in the electromagnetic case, the power is measured integrating the time-average Poynting vector, and it is related to the square of the electric field $|\vec{E}|$ then

$$R = \frac{|\vec{E}_r|^2}{|\vec{E}_i|^2} = \frac{|r\vec{E}_i|^2}{|\vec{E}_i|^2} = |r|^2, \tag{12}$$

where $|\vec{E}_i|$ and $|\vec{E}_r|$ are the incident and reflected fields respectively. In the thermal case, the power is measured by the heat flux, which is linear with the temperature field and the reflectance is

$$R = \frac{|\vec{q}_r|}{|\vec{q}_i|} = \frac{|r\nabla T_i|}{|\nabla T_i|} = |r|. \tag{13}$$

Since $|r|^2 < |r| < 1$, by definition the thermal wave reflectance is bigger than the reflectance of other waves, as will be shown later.

4. Thermal Bragg Mirrors

Optical Bragg mirrors are made of alternate layers of high and low index of refraction materials. The wave nature of the solution of the CVe is explored via a thermal Bragg mirror. We compute the heat flux $\vec{q}(\vec{r}, t) \cdot \hat{n}$ into the layered system.

To extend the definition to thermal wave, we consider three specific materials: Aluminum [43] (Al) and two materials with thermal properties of biological tissue (epidermis and dermis) [13,18,44]. In Table I, the thermal properties of these materials are listed. From the experimental point of view, materials with biological-like responses can be designed with specific thermal properties using gel-phantoms [45].

To illustrate the individual reflection properties of Al and dermis, consider a half-space made of each material in contact with a substrate made of a material with the properties of epidermis. In Fig. 1 we show the reflectance R as a function of the frequency ω for each half-space system. The solid lines correspond to reflectance as $R = |r|$ from Eq. (13) and the dashed lines to $R = |r|^2$ as in other types of waves from Eq. (12). The reflectance from Al (green line) exhibits a weak dependence on frequency reaching the maximum value of $R = 1$ at low frequencies, this material is a good conductor and has a very small relaxation time. The reflectance of dermis (red line) also reaches its maximum ($R = 0.6$) at low frequencies although the relaxation time is larger than Al. This behavior allows us to reduce the frequency domain to take into account ($\omega < 30$ rad/s).

Thermal Bragg mirrors are made of alternate layers of two materials with different thermal admittance. As in the optical case, we expect a frequency dependence on R with high (low) values for different frequency ranges.

Preprints (www.preprints.org) | NOT PEER-REVIEWED | Posted: 12 October 2021 doi:10.20944/preprints202110.0174.v1

Material	Thermal conductivity κ [$Wm^{-1}K^{-1}$]	Specific heat capacity c_V [$J\ kg^{-1}K^{-1}$]	Mass density ρ [Kgm^{-3}]	Response time τ [s]
epidermis (m1)	0.235	3600	1500	1
dermis (m2)	0.445	3300	1116	20
Al	237	921	2707	2×10^{-10}

Table 1: Thermal properties of the materials used in the numerical example of a layered system taken from [13,18]. We will refer to the epidermis as material 1 or m1 and to the dermis as material 2 or m2.

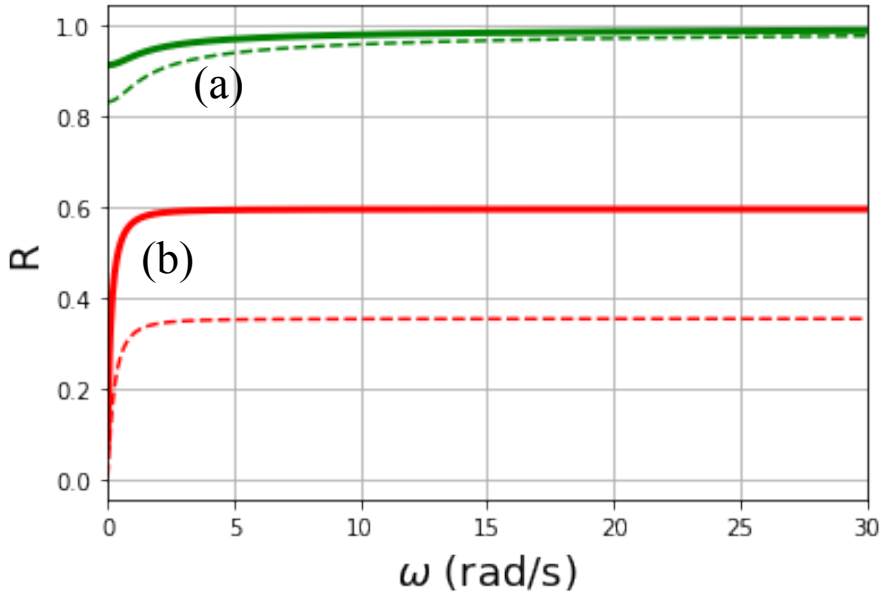

Figure 1. Reflectance R between the medium labeled material 1 and a half space made of Al (a), material 2 (b). The properties of the different materials are given in Table I. As explained in the text, the reflectance for thermal waves is $R = |r|$ (solid), rather than $R = |r|^2$ (dashed) as in other wave phenomena. For metals, that have a very small relaxation time, they behave as perfect reflectors.

As a first case we consider a thermal mirror made of alternate layers of material 2 (dermis) and material 1 (epidermis), shown in Table I. Not including the incident and substrate layers, the unit cell that will be repeated follows the sequence m1-m2. The thickness of each layer is $d = 100\ \mu$m. In Fig. 2(a,b,c) we show the reflectance $R = |r|$ as a function of frequency for different numbers of unit cells. The blue solid line corresponds to R for the finite Bragg mirror and the dashed red line corresponds to the semi-infinite periodic system calculated using Eq. (11). Finally, Fig. 2(d) presents a contour plot of normalized heat flux $\vec{q} \cdot \hat{n}$ into the laminated system, normalized to the incident heat flux of magnitude q_0. The vertical axis is the frequency and in the horizontal axis, the number of unit cells is shown. We observe that frequency regions of high reflectivity correlate with low values of heat flux. Notice that even with a few number of unit cells the rejection-band defined by a high reflectivity is obtained. The rejection-band can be clearly seen in Fig. 2(d) and is delimited by the white-dotted line.

The reflectance in Fig. 2 has the typical form of a periodic system band structure, which ultimately is a result of introducing a delay time in the heat conduction model of Eq. (1). When solving the Fourier equation for the same system, frequency windows of high or low reflectance do not appear, instead a monotonous behavior for the reflectance and heat flux is obtained, as we show in Fig. 3. In this figure the same m1-m2 sequence was used as in the CV case and represents the diffusive limit for the Fig. 2(d).

Preprints (www.preprints.org) | NOT PEER-REVIEWED | Posted: 12 October 2021 doi:10.20944/preprints202110.0174.v1

We emphasize that the heat flux behavior in a periodic system which is analogous to the energy band structure of electrons in solids is a consequence of the CVe and it is not predicted by Fourier's law, as is shown in Fig. 3. Furthermore, the frequency dependence on the reflectance is only obtained when solving the CVe and not the Fourier case.

For this reason, an experimental setup similar to the layered system studied in this work could be used to verify or discard the existence of thermal waves.

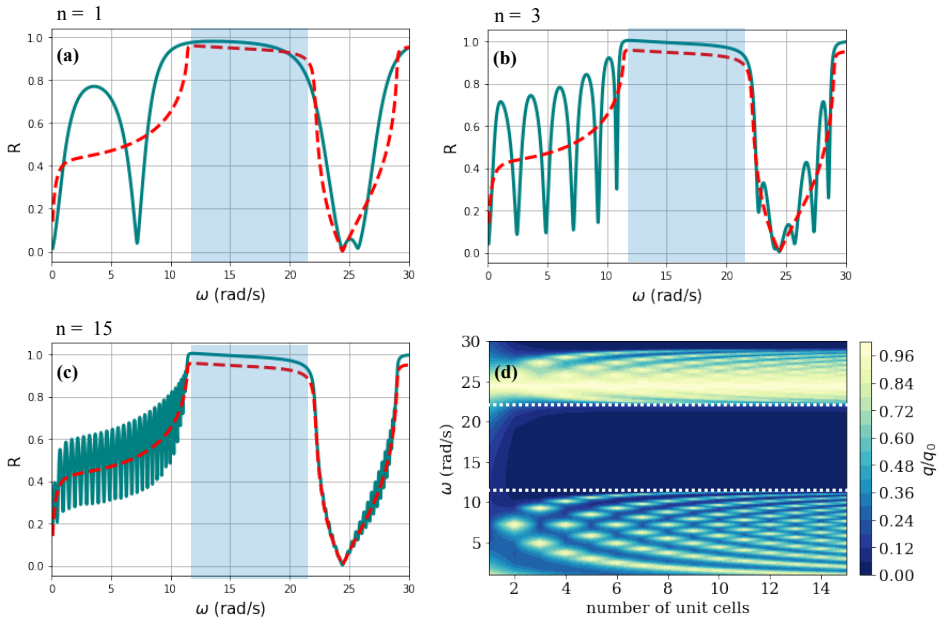

Figure 2. For a system with unit cells made of alternating layers of material 1 and material 2 (see Table I) and both of thickness $d = 100$ μm, we present in (a,b,c) the reflectance $R = |r|$ as a function of frequency for different numbers of unit cells n in a solid line, the dashed line represents the semi-infinite periodic case. In Fig.(d) the heat flux into the system at $x = 0$ is shown as function of frequency and n. The flux is normalized to the incident flux q_0. The stop-band is seen even for a few number of unit cells. The dotted lines indicate the position of the first stop-band for the semi-infinite crystal.

Preprints (www.preprints.org) | NOT PEER-REVIEWED | Posted: 12 October 2021 doi:10.20944/preprints202110.0174.v1

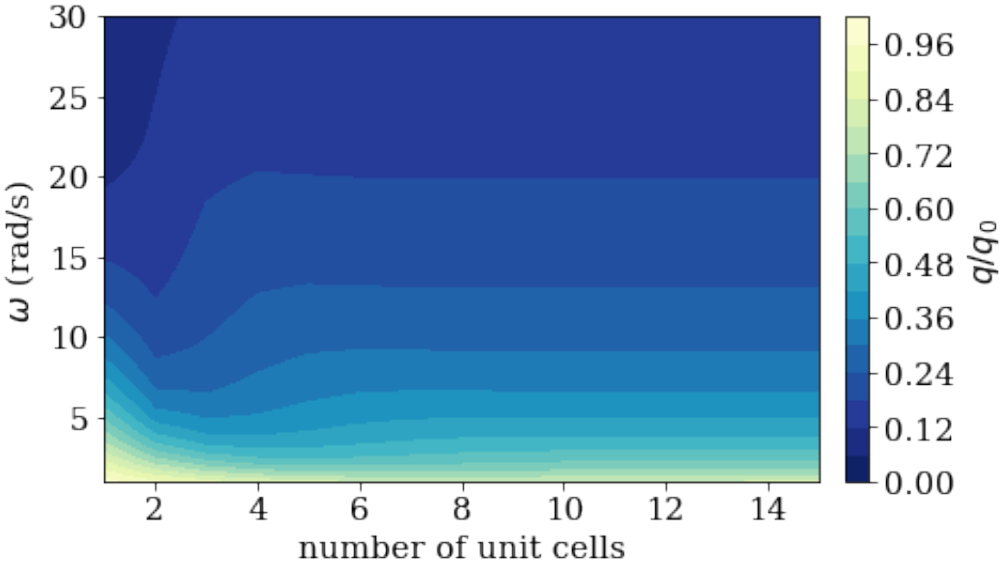

Figure 3. Normal heat flux in a contour plot for a system with unit cells made of alternating layers of material 1 and material 2 assuming they have relaxation time equal to zero which corresponds to the Fourier law case.

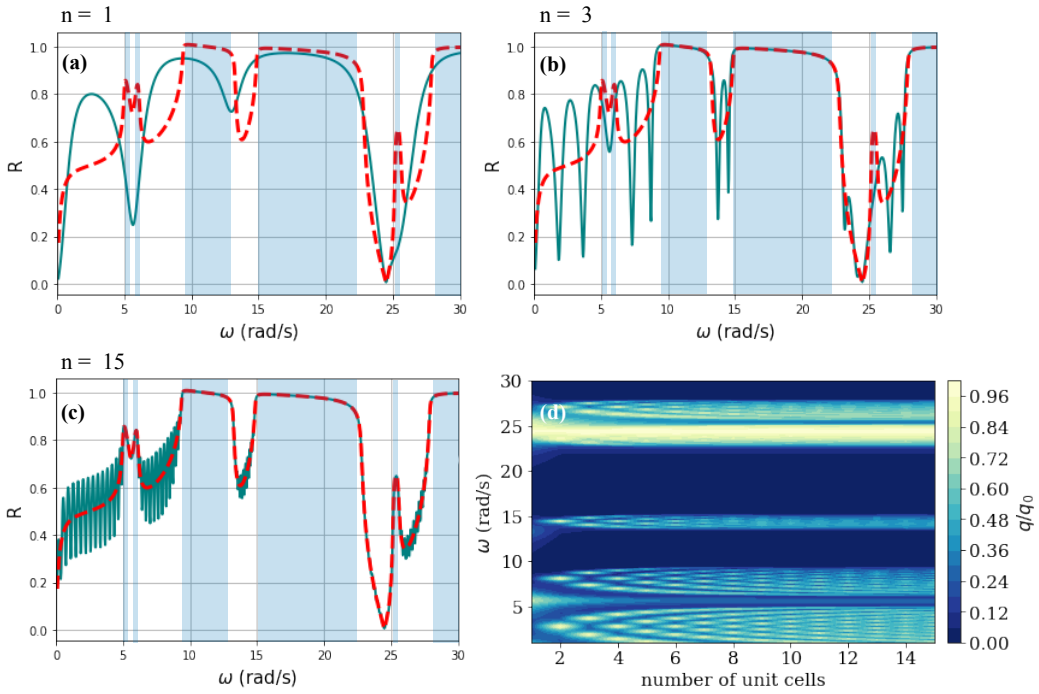

Figure 4. (a) - (c) Reflectance and normalized (d) heat flux of a system with unit cell m1-m2-Al-m2 (1-2-Al-2). Layers of Material 1 and 2 have a thickness of $d = 100\mu$m while for that of Al $d_{al} = 1\mu$m.

4.1. Tuning of the thermal reflectance

Having the stop or rejection band in a frequency window opens the possibility of fine-tuning the thermal reflectance and heat flux by modifying the unit-cells. For example if we have the unit-cell constructed as m1-m2-Al-m2, where the second layer of Material 1 is replaced by an Aluminum layer of thickness to $0.01d = 1\mu$m. In this case, the reflectance and normalized heat flux are presented in Fig. 4.

 doi:10.20944/preprints202110.0174.v1

As expected, new states appear and are indicated by shaded rectangles in Fig.4 (a,b,c). We observe that reflectance for $n = 1$ and $n = 3$, shows a good agreement with the semi-infinite periodic medium, such that there are well defined frequency windows of high reflectance. However for few unit cells, the narrowest frequency windows are not defined yet and appear until we use 15 unit cells as is shown in Figs.4 (c), this is what we mean as fine-tuning of heat flux.

Metals have negligible relaxation times, follow Fourier's law and are malleable, thus have the advantage of being easy to fabricate with a well defined thickness within the periodic structure. A comparison of Figs. 2 and 4 shows to what degree the heat flux can be modified simply by adding an aluminum layer. The high reflectance region is subdivided into four narrower high reflectance regions. The thermal Bragg mirrors result from the contrast between the thermal properties of layer materials and the number of unit cells, analogue to the refractive index combination of optics Bragg mirrors.

5. Conclusions

In this paper, we showed the possibility of constructing Bragg mirrors for thermal waves that are a solution to the Cattaneo-Vernotte equation, it cannot be generated using Fourier's law to model heat conduction. The mirrors are made of alternate layers of two different materials yielding a reflectance definition different to other waves, it reaches values higher than 90%.

The response of the thermal Bragg mirrors is changed by introducing an aluminum layer in the unit cell. In this case, regions of high reflectance are obtained. At the frequencies of these bands, no heat flows into the mirror and can be referred to as stopbands. The counterpart result can be used to generate regions of low reflectance where a large heat flux into the mirror is possible, identified as passbands.

Besides being a suitable system to demonstrate the wave nature of the heat flux and temperature for some non-Fourier materials, Bragg mirrors can be effective thermal shields by a reasonable design of the mirror and materials.

To our knowledge, the body of experimental work has been limited to homogeneous systems and no experimental data on thermal Bragg mirrors is available for a comparison with our results that show the feasibility of constructing such mirrors. The wave-like nature of the temperature and heat flux derived from the Cattaneo-Vernotte equation is an approximation with many issues still under discussion in the literature. The proposed Bragg mirror will be a simple approach to determine the feasibility of the wave-like nature of the solutions and new possibilities for thermal management using analogies to other wave phenomena such as electromagnetic [29,46,47] or acoustic waves [39,48,49].

Acknowledgments: We appreciate the valuable comments of S. G. Castillo-López. Partial support from DGAPA-UNAM Grant IN110819 and CONACyT A1-S-10537.

Conflicts of Interest: The authors declare no conflict of interest.

References

1. Cattaneo, C. *Sulla Conduzione Del Calore*; Springer Berlin Heidelberg: Berlin, Heidelberg, 2011; pp. 485–485.
2. Vernotte, P. Les paradoxes de la théorie continue de lequation de la chaleur. *C. R. Acad. Sci. Paris* **1958**, *246*, 3154–3155.
3. Kaminski, W. Hyperbolic Heat Conduction Equation for Materials With a Nonhomogeneous Inner Structure. *J. Heat Trans.* **1990**, *112*, 555–560.
4. Cassol, G.O.; Dubljevic, S. Hyperbolicity of the heat equation. *IFAC-PapersOnLine* **2019**, *52*, 63 – 67. 3rd IFAC Workshop on Thermodynamic Foundations for a Mathematical Systems Theory TFMST 2019.
5. Joseph, D.D.; Preziosi, L. Heat waves. *Reviews of Modern Physics* **1989**, *61*, 41.
6. Marín, E.; Vaca-Oyola, L.; Delgado-Vasallo, O. On thermal waves velocity: some open questions in thermal waves' physics. *Revista mexicana de física E* **2016**, *62*, 1–4.
7. Gandolfi, M.; Benetti, G.; Glorieux, C.; Giannetti, C.; Banfi, F. Accessing temperature waves: A dispersion relation perspective. *Int. J. Heat and Mass Trans.* **2019**, *143*, 118553.
8. Roetzel, W.; Putra, N.; Das, S.K. Experiment and analysis for non-Fourier conduction in materials with non-homogeneous inner structure. *International Journal of Thermal Sciences* **2003**, *42*, 541 – 552.

9. Graßmann, A.; Peters, F. Experimental investigation of heat conduction in wet sand. *Heat and Mass Transfer* **1999**, *35*, 289–294. doi:10.1007/s002310050326.
10. Jaunich, M.; Raje, S.; Kim, K.; Mitra, K.; Guo, Z. Bio-heat transfer analysis during short pulse laser irradiation of tissues. *Int. J. Heat Mass Transf.* **2008**, *51*, 5511 – 5521. Biomedical-Related Special Issue.
11. Mandhukar, A.; Park, Y.; Kim, W.; Sunaryanto, H.J.; Berlin, R.; Chamorro, L.P.; Bentsman, J.; Ostoja-Starzewski, M. Heat conduction in porcine muscle and blood: experiments and time-fractional telegraph equation model. *J. R. Soc. Interface* **2019**, *16*, 20190726.
12. K. Mitra, S. Kumar, A.V.; Moallemi, M. Experimental Evidence of Hyperbolic Heat Conduction in Processed Meat. *J. Heat Transfer* **1995**, *117*, 568–573.
13. Xu, F.; Seffen, K.A.; Lu, T.J. Non-Fourier analysis of skin biothermomechanics. *Int. J. Heat Mass Transf.* **2008**, *51*, 2237 – 2259.
14. Kovács, R.; Ván, P. Generalized heat conduction in heat pulse experiments. *Int. J. Heat Mass Transf.* **2015**, *83*, 613 – 620.
15. Ahmadikia, H.; Fazlali, R.; Moradi, A. Analytical solution of the parabolic and hyperbolic heat transfer equations with constant and transient heat flux conditions on skin tissue. *Int. J. Heat Mass Transf.* **2012**, *39*, 121 – 130.
16. Beardo, A.; López-Suárez, M.; Pérez, L.A.; Sendra, L.; Alonso, M.I.; Melis, C.; Bafaluy, J.; Camacho, J.; Colombo, L.; Rurali, R.; Alvarez, F.X.; Reparaz, J.S. Observation of second sound in a rapidly varying temperature field in Ge. *Science Advances* **2021**, *7*, eabg4677, [https://www.science.org/doi/pdf/10.1126/sciadv.abg4677]. doi:10.1126/sciadv.abg4677.
17. Farhat, M.; Guenneau, S.; Chen, P.Y.; Alù, A.; Salama, K.N. Scattering Cancellation-Based Cloaking for the Maxwell-Cattaneo Heat Waves. *Phys. Rev. Applied* **2019**, *11*, 044089. doi:10.1103/PhysRevApplied.11.044089.
18. Chen, A.L.; Li, Z.Y.; Ma, T.X.; Li, X.S.; Wang, Y.S. Heat reduction by thermal wave crystals. *Int. J. Heat and Mass Transf.* **2018**, *121*, 215–222.
19. Gandolfi, M.; Giannetti, C.; Banfi, F. Temperonic crystal: A superlattice for temperature waves in graphene. *Phys. Rev. Lett.* **2020**, *125*, 265901.
20. Ordóñez-Miranda, J.; Alvarado-Gil, J. Effective thermal properties of layered systems under the parabolic and hyperbolic heat conduction models using pulsed heat sources. *J. Heat Transf.* **2011**, *133*.
21. Vázquez, F.; Ván, P.; Kovács, R. Ballistic-Diffusive Model for Heat Transport in Superlattices and the Minimum Effective Heat Conductivity. *Entropy* **2020**, *22*. doi:10.3390/e22020167.
22. Estrada-Wiese, D.; del Río, J.A.; de la Mora, M.B. Heat transfer in photonic mirrors. *Journal of Materials Science: Materials in Electronics* **2014**, *25*, 4348–4355. doi:10.1007/s10854-014-2172-z.
23. Borca-Tasciuc, T.; Liu, W.; Liu, J.; Zeng, T.; Song, D.W.; Moore, C.D.; Chen, G.; Wang, K.L.; Goorsky, M.S.; Radetic, T.; Gronsky, R.; Koga, T.; Dresselhaus, M.S. Thermal conductivity of symmetrically strained Si/Ge superlattices. *Superlattices and Microstructures* **2000**, *28*, 199 – 206.
24. Chen, G.; Neagu, M. Thermal conductivity and heat transfer in superlattices. *App. Phys. Lett.* **1997**, *71*, 2761–2763.
25. Esquivel-Sirvent, R.; Cocoletzi, G. Band structure for the propagation of elastic waves in superlattices. *J. Acous. Soc. Am* **1994**, *95*, 86–90.
26. El Boudouti, E.H.; Djafari-Rouhani, B. Acoustic waves in finite superlattices. *Phys. Rev. B* **1994**, *49*, 4586–4592.
27. de la Cruz, G.G. Bulk and surface plasmons in graphene finite superlattices. *Superlatt. Microstruct.* **2019**, *125*, 315–321.
28. Jena, S.; Tokas, R.B.; Thakur, S.; Udupa, D.V. Tunable mirrors and filters in 1D photonic crystals containing polymers. *Phys. E: Low-dimensional Systems and Nanostructures* **2019**, *114*, 113627.
29. Al-sheqefi, F.; Belhadj, W. Photonic band gap characteristics of one-dimensional graphene-dielectric periodic structures. *Superlattices Microstruct.* **2015**, *88*, 127 – 138.
30. Kone, I.; Domingue, F.; Reinhardt, A.; Jacquinot, H.; Borel, M.; Gorisse, M.; Parat, G.; Casset, F.; Pellissier-Tanon, D.; Carpentier, J.; others. Guided acoustic wave resonators using an acoustic Bragg mirror. *App. Phys. Lett.* **2010**, *96*, 223504.
31. Herrera, L. Causal heat conduction contravening the fading memory paradigm. *Entropy* **2019**, *21*, 950.
32. Barletta, A.; Zanchini, E. Hyperbolic heat conduction and local equilibrium: a second law analysis. *International Journal of Heat and Mass Transfer* **1997**, *40*, 1007–1016.
33. Özısık, M.N. *Heat Conduction*; Wiley-Interscience publication, Wiley, 1993.
34. Bockh, P.V.; Wetzel, T. *Heat Transfer*, 3 ed.; Vol. 4, *10*, Springer, 1993.
35. Ostoja-Starzewski, M. A derivation of the Maxwell–Cattaneo equation from the free energy and dissipation potentials. *Int. J. Eng. Sci.* **2009**, *47*, 807 – 810.
36. Green, D.R. Thermal Surface Impedance for Plane Heat Waves in Layered Materials. *J. App. Phys.* **1966**, *37*, 3095–3099.
37. Li, B.c.; Zhang, S.y. The effect of interface resistances on thermal wave propagation in multi-layered samples. *J. Phys. D: App. Phys.* **1997**, *30*, 1447.
38. Pérez-Álvarez, R.; García-Moliner, F. *Transfer Matrix, Green Function and related techniques: Tools for the study of multilayer heterostructures*; Publicacions de la Universitat Jaume I, 2004.
39. Esquivel-Sirvent, R.; Cocoletzi, G.H. Band structure for the propagation of elastic waves in superlattices. *J. Ac. Soc. Am.* **1994**, *95*, 86–90. doi:10.1121/1.408301.
40. Patel, H.A.; Garde, S.; Keblinski, P. Thermal resistance of nanoscopic liquid- liquid interfaces: dependence on chemistry and molecular architecture. *Nano Letters* **2005**, *5*, 2225–2231.

41. Hasan, M.R.; Vo, T.Q.; Kim, B. Manipulating thermal resistance at the solid–fluid interface through monolayer deposition. *RSC Adv.* **2019**, *9*, 4948–4956.
42. Knobel, R. *An introduction to the mathematical theory of waves*; Vol. 3, American Mathematical Soc., 2000.
43. Ranut, P.; Nobile, E. On the effective thermal conductivity of metal foams. *J. Phys.: Conf. Series* **2014**, *547*, 012021. doi:10.1088/1742-6596/547/1/012021.
44. Kundu, B. Exact analysis for propagation of heat in a biological tissue subject to different surface conditions for therapeutic applications. *App. Math. Comp.* **2016**, *285*, 204 – 216. doi:https://doi.org/10.1016/j.amc.2016.03.037.
45. Oana I. Craciunescu, Laurens E. Howle, S.T.C. Experimental evaluation of the thermal properties of two tissue equivalent phantom materials. *Int. J. Hypertherm.* **1999**, *15*, 509–518.
46. Sánchez, A.; Porta, A.V.; Orozco, S. Photonic band-gap and defect modes of a one-dimensional photonic crystal under localized compression. *J. App. Phys.* **2017**, *121*, 173101.
47. Scalora, M.; Bloemer, M.J.; Pethel, A.S.; Dowling, J.P.; Bowden, C.M.; Manka, A.S. Transparent, metallo-dielectric, one-dimensional, photonic band-gap structures. *J. App. Phys.* **1998**, *83*, 2377–2383.
48. Kushwaha, M.S.; Halevi, P. Band-gap engineering in periodic elastic composites. *App. Phys. Lett.* **1994**, *64*, 1085–1087. doi:10.1063/1.110940.
49. Esquivel-Sirvent, R.; Noguez, C. Theory of the acoustic signature of topological and morphological defects in SiC/porous SiC laminated ceramics. *J. App. Phys.* **1997**, *82*, 3618–3620.